Supporting Information

Synthesis of Fine Cubic $Li_7La_3Zr_2O_{12}$ Powders in Molten LiCl-KCl Eutectic and Facile Densification by Reversal of Li^+/H^+ Exchange

J. Mark Weller, Justin A. Whetten, Candace K. Chan*

Materials Science and Engineering, School for Engineering of Matter, Transport and Energy, Arizona State University, Tempe, AZ 85287-6106

Corresponding Author

* E-mail: candace.chan@asu.edu, Phone: (480) 727-8614.

Electrochemical Impedance Spectroscopy Fitting

In general, the impedance spectrum of a solid ionic conductor is expected to have contributions corresponding to the contact (i.e., electrode) impedance, bulk (i.e., grain volume) impedance, and grain boundary impedance. However, for LLZO, the grain boundary impedance is often negligible compared to the bulk impedance at room temperature, particularly in well-densified pellets (i.e., those with low porosity and transgranular fracture surfaces) (1). This means that it is often difficult to resolve the bulk and grain boundary impedances unless measurements are performed at low temperatures (2, 3).

Further, the insufficient data points at the high frequencies to make a full semicircle can make fitting and interpretation of the impedance data challenging. In our case, we found that fitting the impedance data to the equivalent circuit $(R_1Q_1)(R_2Q_2)(R_3Q_3)$ gave the smallest X^2 values. The fitting results are shown in Table S2. The distance between the real and simulated data is represented by X^2 , X^2 weighted by the impedance modulus |Z|, and the normalized expression of X^2, $X/(N)^{1/2}$, which is independent of the numbers of points and is equivalent to an error (4).

In each case, the bulk ionic conductivity, σ (S/cm), was determined from the R_2 values, the pellet thickness (d), and the pellet cross-sectional area (A) using Equation S1:

$$\sigma = \frac{d}{R_2 A} \qquad \text{(S1)}$$

Supporting Tables

Table S1. Reaction temperature and duration used for exploratory MSS syntheses without added dopants. The corresponding XRD patterns for the products obtained in these experiments are shown in Figure S2.

Experiment #	Conditions	Results
1	500°C 1 hour	LaOCl
2	500°C 2 hours	LaOCl
3	500°C 3 hours	LaOCl
4	600°C 1 hour	LaOCl + LZO
5	600°C 2 hours	LaOCl + LZO
6	600°C 3 hours	LaOCl + LZO
7	700°C 1 hour	LaOCl + LZO
8	700°C 2 hours	LaOCl + LZO
9	700°C 3 hours	LaOCl + LZO
10	800°C 1 hour	LZO
11	800°C 2 hours	LZO
12	800°C 3 hours	LZO
13	900°C 1 hour	LZO
14	900°C 2 hours	LZO
15	900°C 3 hours	LZO + **c-LLZO**
16	900°C 6 hours	**c-LLZO**

Table S2. Z Fit parameters for EIS data of (**a**) ALLZO pellet (10% LiOH added, 18 hr sinter), (**b**) GLLZO pellet (10% LiOH added, 12 hr sinter), (**c**) GLLZO pellet (3% LiOH added, 6 hr sinter)

	a) **ALLZO (10%)**	b) **GLLZO (10%)**	c) **GLLZO (3%)**
Q_1	$44.61e^{-9}$ F	$9.611e^{-9}$ F	$0.214e^{-6}$ F
a_1	0.862	0.773	0.787
R_1	466.8 Ω	224.8 Ω	145.2 Ω
Q_2	$0.183e^{-9}$ F	$26.45e^{-9}$ F	$2.263e^{-9}$ F
a_2	0.985	0.597	0.730
R_2	**1261 Ω**	**582.1 Ω**	**472.5 Ω**
Q_3	$0.347e^{-6}$ F	$1.283e^{-6}$ F	$0.502e^{-6}$ F
a_3	0.683	0.603	0.703
R_3	307734 Ω	50,434 Ω	58837 Ω
$\boldsymbol{\chi}^2/\lvert Z\rvert$	$3.12e^{-3}$	$3.30e^{-3}$	$9.27e^{-4}$
$\boldsymbol{\chi}^2$	5505	2584	302.4
$\mathbf{X}/\sqrt{(N)}$	6.423	7.417	2.785
Thickness	0.0906 cm	0.0481 cm	0.0585 cm
Area	0.312 cm^2	0.256 cm^2	0.3338 cm^2
σ	**0.230 mS cm^{-1}**	**0.323 mS cm^{-1}**	**0.371 mS cm^{-1}**

Supporting Figures

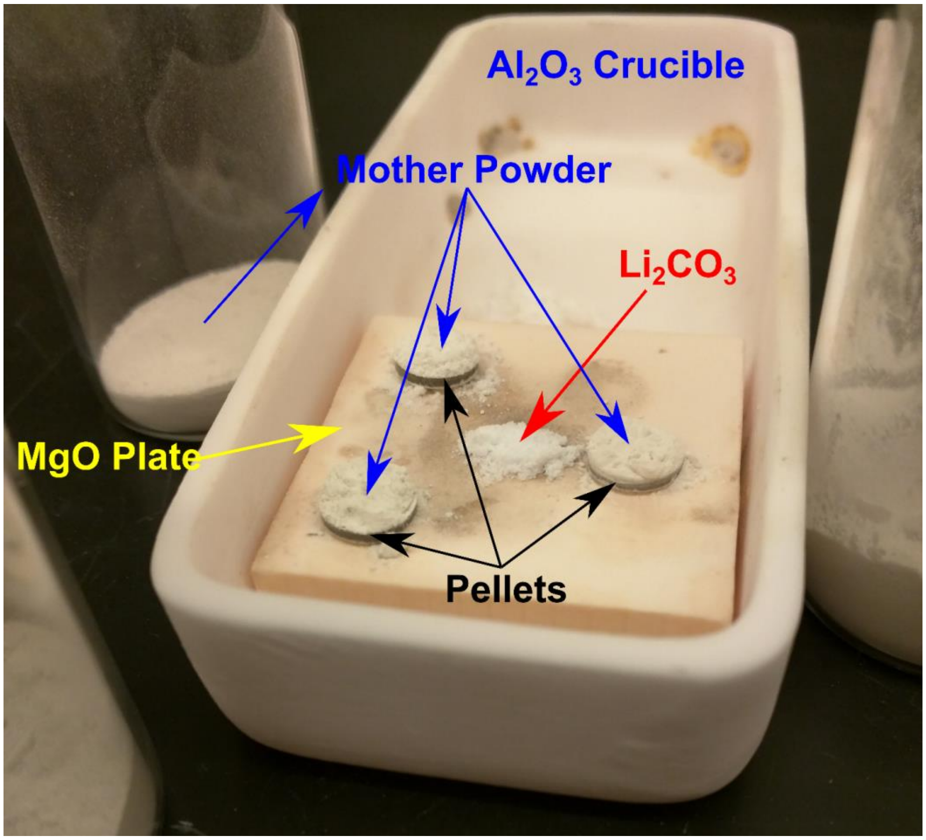

Figure S1. Photograph of typical pellet configuration for sintering. An MgO plate is set inside of a larger Al_2O_3 crucible. Then, mother powder is placed on the MgO plate. The pressed green pellets are placed on top of the mother powder and then coated with more mother powder. A small amount of Li_2CO_3 is placed on the MgO crucible in the middle of the pellets to provide Li-rich vapor during sintering. Finally, the entire assembly is covered in an Al_2O_3 lid.

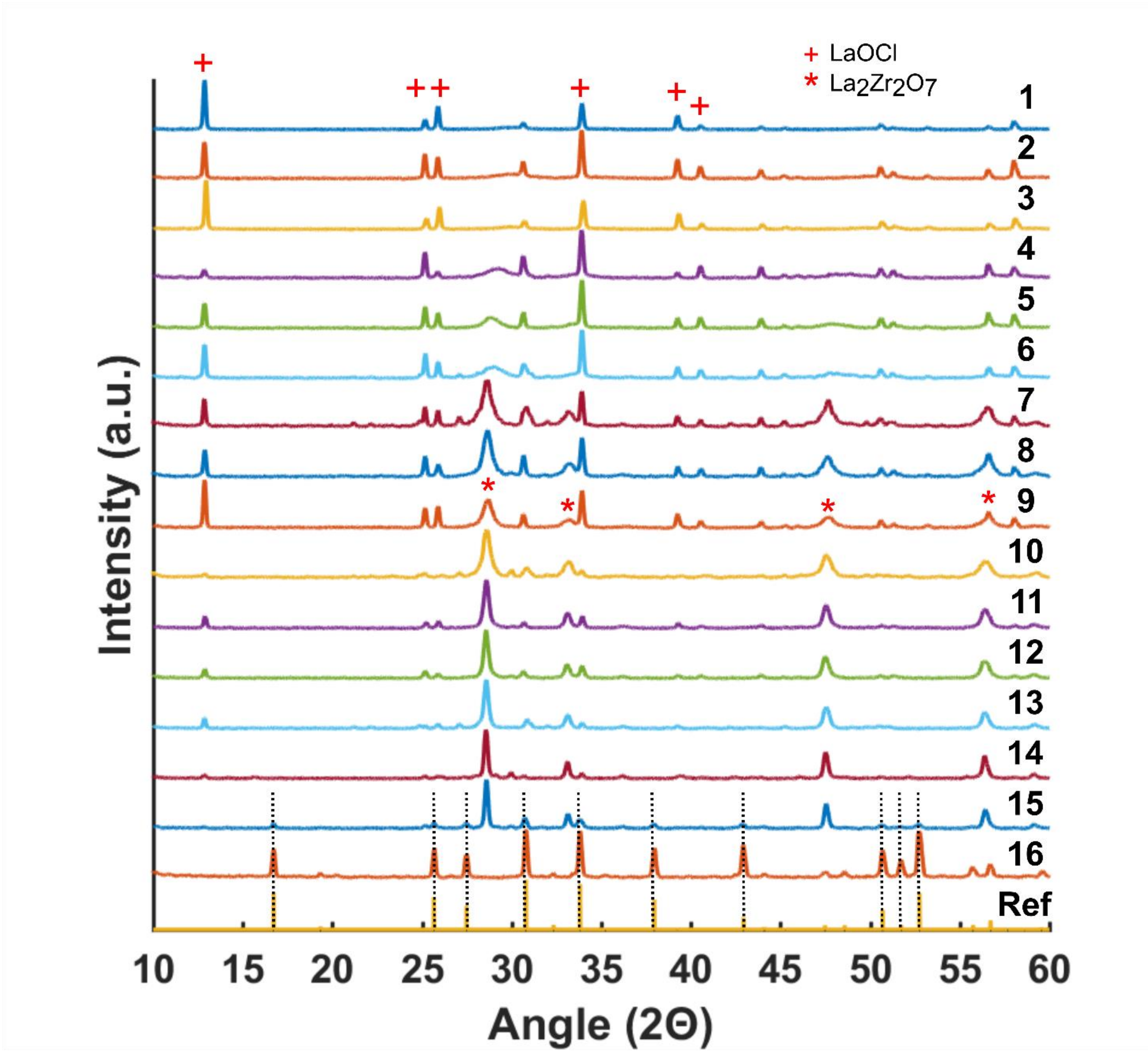

F**igure S2**. XRD patterns corresponding to the experimental parameters in Table S1, with various synthesis times and temperatures ranging from 1 to 3 hr and 500 °C to 900 °C. The LLZO reference pattern is shown at the bottom.

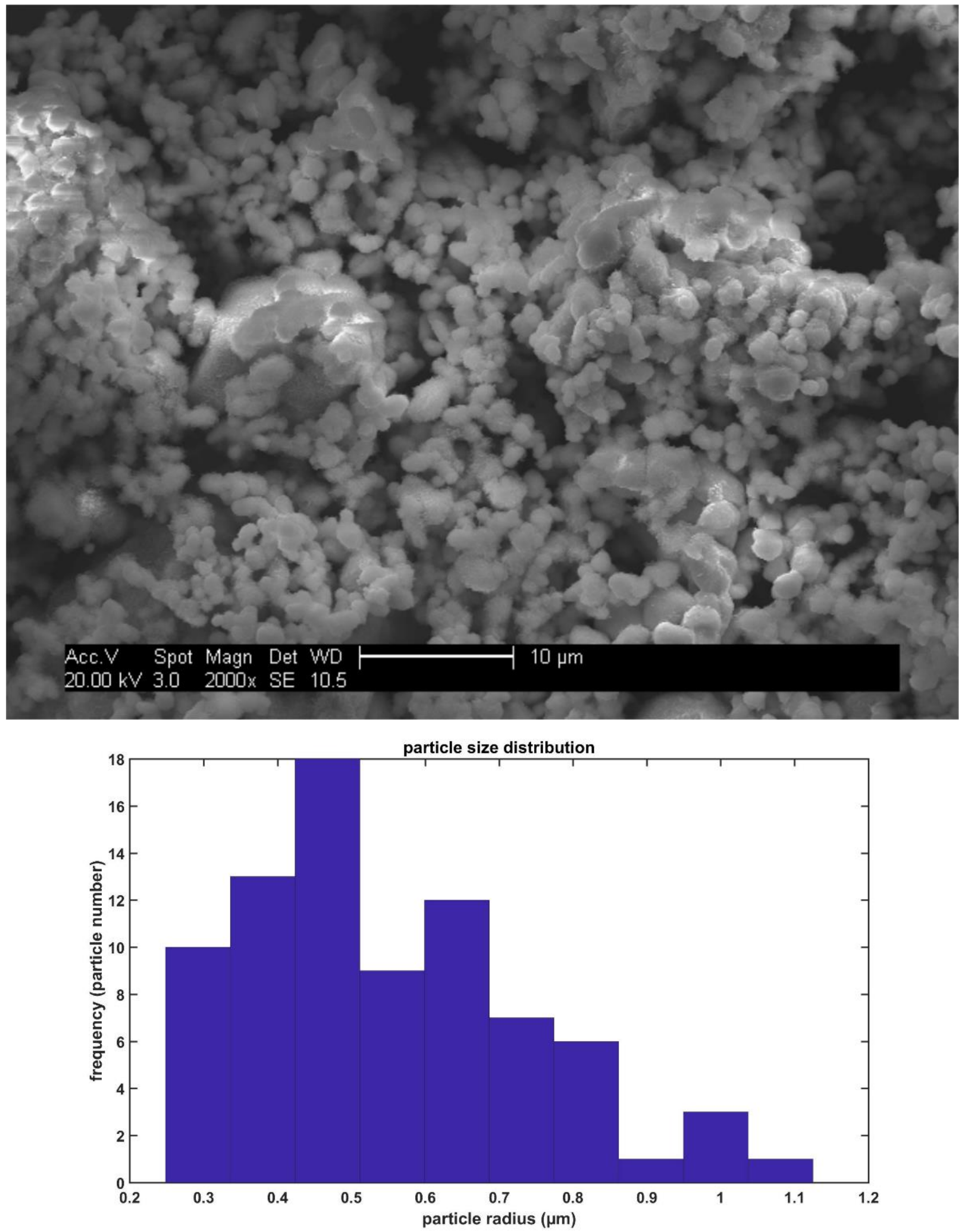

Figure S3. (**top**) SEM image of undoped c-LLZO powder synthesized at 900°C for 4 hr, (**bottom**) histogram showing particle radius distribution

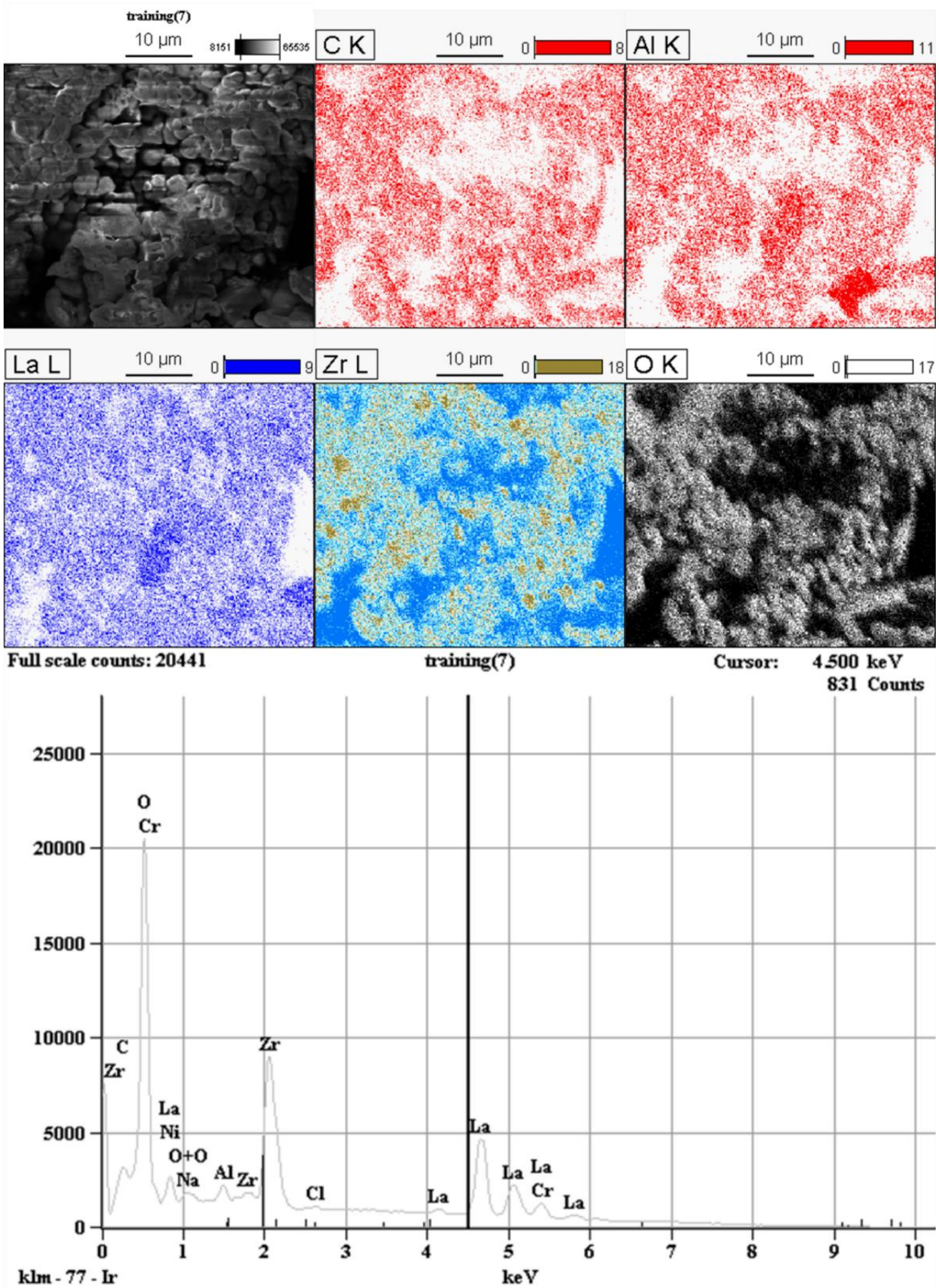

Figure S4. EDS maps and spectrum of ALLZO powders, illustrating uniform distribution of Al.

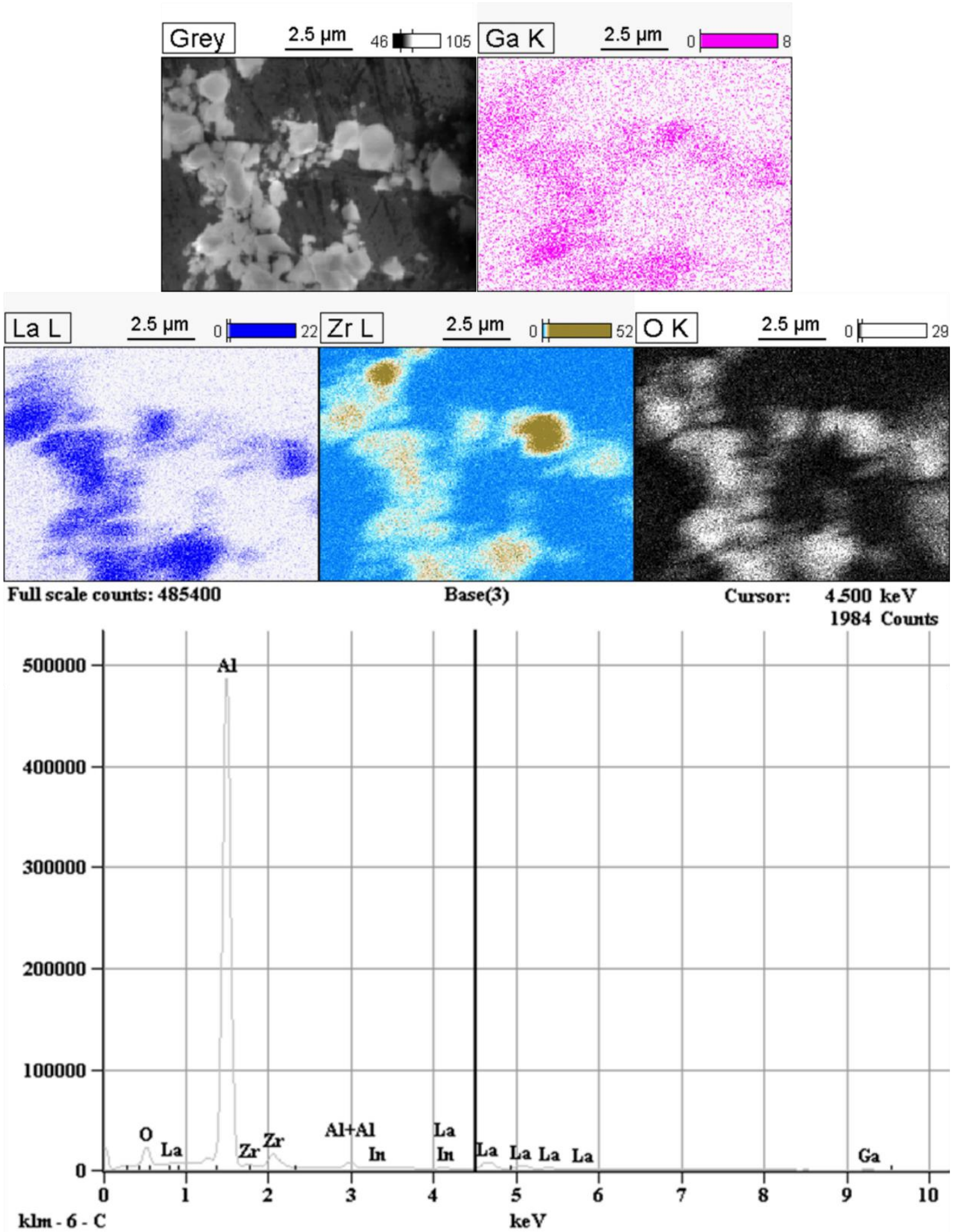

Figure S5. EDS maps and spectrum of GLLZO powders, illustrating uniform distribution of Ga (note that the Al-signal in the EDS spectrum is from the SEM substrate).

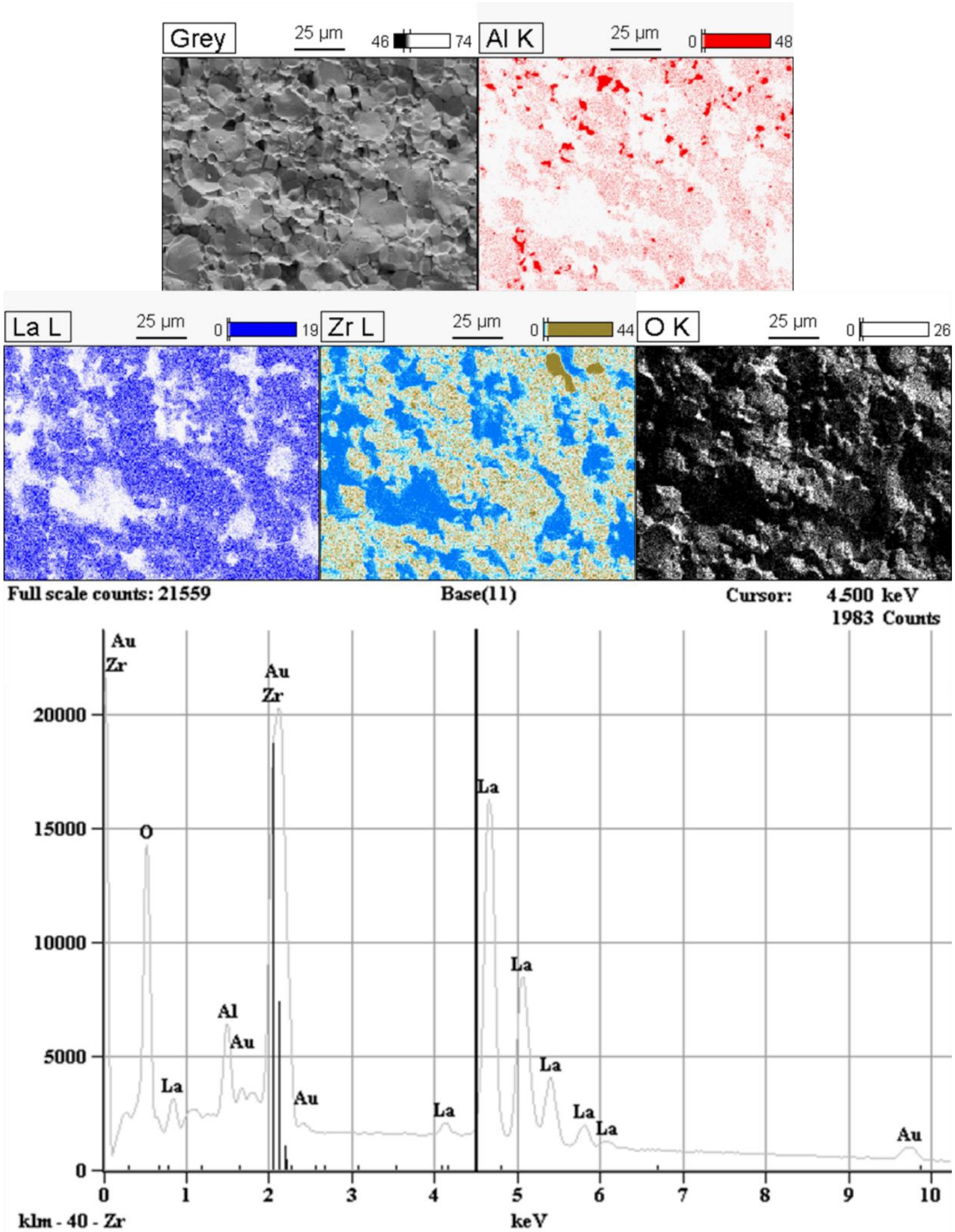

Figure S6. EDS maps and spectrum of ALLZO pellet fracture surface, illustrating uniform distribution of A. Note that presence of Au signal is due to sputtered layer to minimize charging, and regions of higher intensity seen particularly in the Al K map may be due to X-Ray takeoff angle matching the detector acceptance angle or presence of Al-rich phases

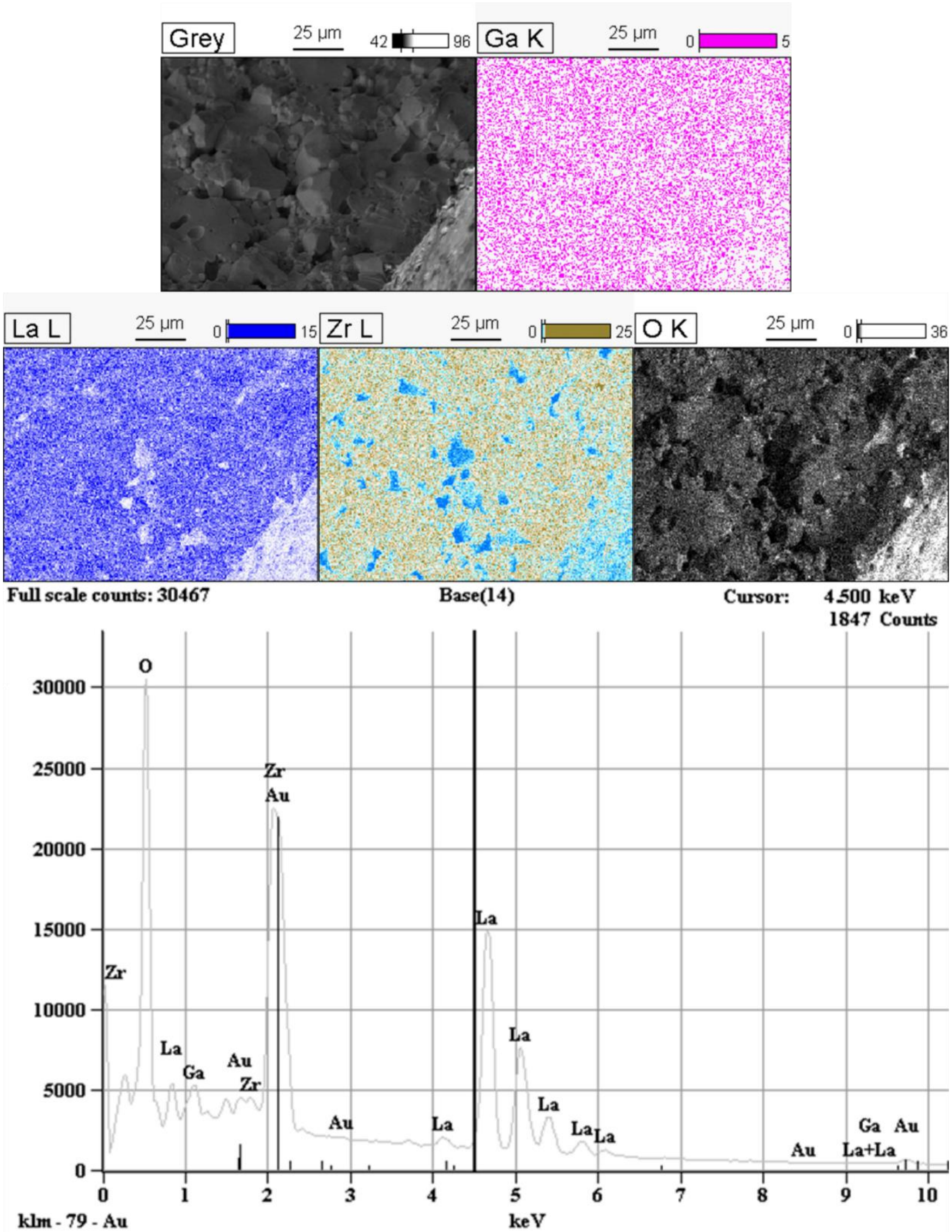

Figure S7. EDS maps and spectrum of GLLZO pellet fracture surface, illustrating uniform distribution of Ga (presence of Au signal is due to sputtered layer to minimize charging).

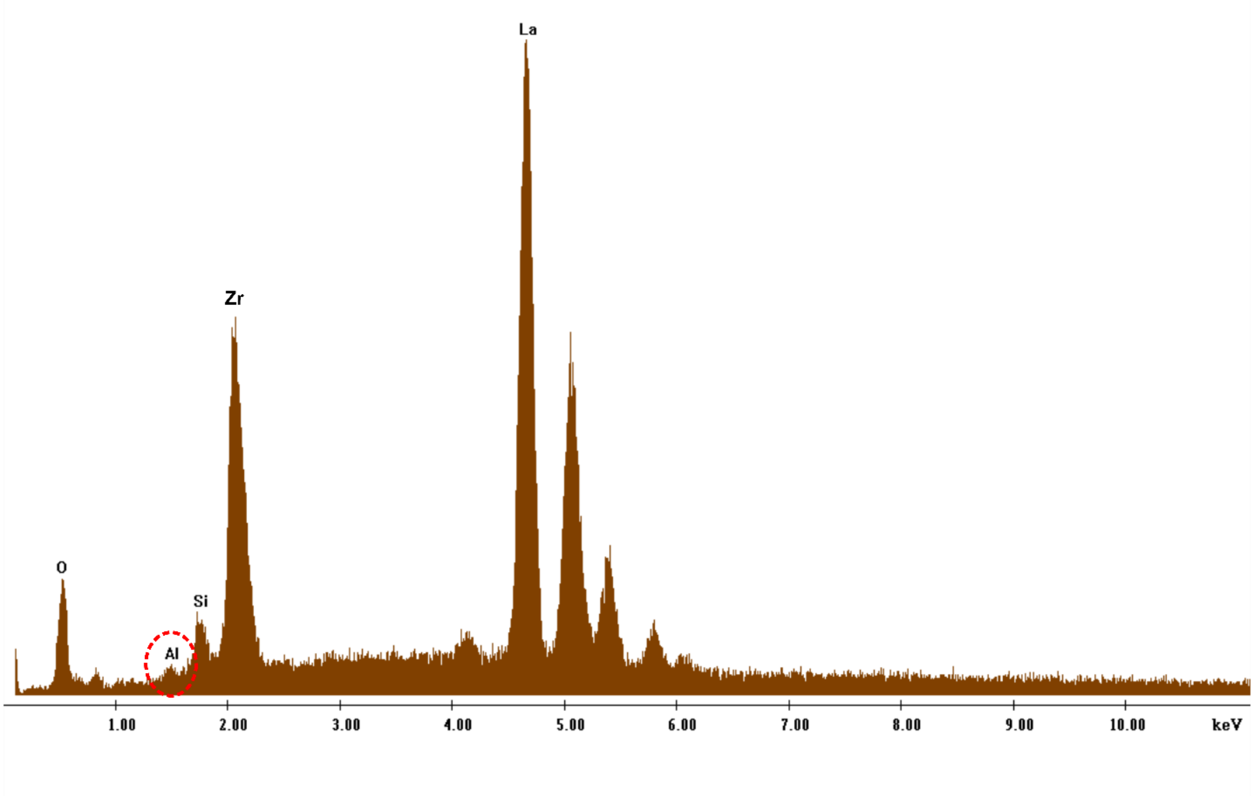

Figure S8. EDS spectrum of c-LLZO experiment # 16 (6 hr reaction time at 900 °C). A small amount of Al signal can be seen, suggesting that some adventitious Al-doping from the alumina crucible is possible. However, the relative signal level is substantially less than that of the intentionally Al-doped LLZO (see Figure S6 EDS spectrum)

References:

(1) Yi, E.; Wang, W.; Kieffer, J.; Laine, R.M. Key parameters governing the densification of cubic-$Li_7La_3Zr_2O_{12}$ Li^+ conductors. *J. Power Sources* 2017, 352, 156-164.

(2) Tenhaeff, W.E.; Rangasamy, E.; Wang, Y.; Sokolov, A.P.; Wolfenstine, J.; Sakamoto, J.; Dudney, N.J. Resolving the grain boundary and lattice impedance of hot-pressed $Li_7La_3Zr_2O_{12}$ garnet electrolytes. *Chem. Electro. Chem.* 2014, 1, 375-378.

(3) Rettenwander, D.; Redhammer, G.; Preishuber-Pflügl, F.; Cheng, L.; Miara, L.; Wagner, R.; Welzl, A.; Suard, E.; Doeff, M.M.; Wilkening, M.; Fleig, J.; Amthauer, G. Structural and electrochemical consequences of Al and Ga cosubstitution in $Li_7La_3Zr_2O_{12}$ solid electrolytes. *Chem. Mater*. 2016, 28, 2384–2392.

(4) BT-Lab® & EC-Lab® Software Analysis and Data Process, BioLogic Science Instruments, Seyssinet-Pariset, France, 2017.